

Coexistence of different electronic phases in the $K_{0.8}Fe_{1.6}Se_2$ superconductor: a bulk-sensitive hard x-rays spectroscopy study.

L. Simonelli,¹ N.L. Saini,² M. Moretti Sala,¹ Y. Mizuguchi,³ Y. Takano,³ H. Takeya,³ T. Mizokawa,⁴ and G. Monaco¹

¹*European Synchrotron Radiation Facility, BP220, F-38043 Grenoble Cedex, France*

²*Dipartimento di Fisica, Università di Roma "La Sapienza" - P. le Aldo Moro 2, 00185 Roma, Italy, EU*

³*National Institute for Materials Science, 1-2-1 Sengen, Tsukuba 305-0047, Japan and JST-TRIP, 1-2-1 Sengen, Tsukuba 305-0047, Japan*

⁴*Department of Physics, University of Tokyo, 5-1-5 Kashiwanoha, Kashiwa, Chiba 277-8561, Japan and Department of Complexity Science and Engineering, University of Tokyo, 5-1-5 Kashiwanoha, Kashiwa, Chiba 277-8561, Japan*

(Dated: March 8, 2013)

We have studied electronic and magnetic properties of the $K_{0.8}Fe_{1.6}Se_2$ superconductor by x-ray absorption and emission spectroscopy. Detailed temperature dependent measurements along with a direct comparison with the binary FeSe system have revealed coexisting electronic phases: a majority phase with high spin ^{3+}Fe state and a minority phase with intermediate spin ^{2+}Fe state. The effect of high temperature annealing suggests that the compressed phase with lower spin ^{2+}Fe state is directly related with the high T_c superconductivity in the title system. The results clearly underline glassy nature of superconductivity in the electronically inhomogeneous $K_{0.8}Fe_{1.6}Se_2$, similar to the superconductivity in granular phases.

PACS numbers: 74.25.Jb, 74.70.Xa, 74.81.Bd

1. INTRODUCTION

The discovery of superconductivity in binary FeSe (11-type) chalcogenide has been an important finding to progress in the understanding of iron-based superconductors¹. The 11-type chalcogenides have been regarded as model systems to explore the fundamental electronic structure of the iron-based superconductors since, unlike the more common $RFeAsO$ ($R = La, Nd, Pr, Sm, Gd$) and $(Ba, Sr)Fe_2As_2$ pnictides, they lack the spacer layers and hence the central role played by the Fe-Fe plane with interacting anions (pnictogen/chalcogen) can be distinctly identified.

Very recently, FeSe layers have been successfully intercalated by alkaline atoms, with intercalated $A_xFe_{2-y}Se_2$ ($A = K, Rb, Cs$) system showing superconductivity up to 32 K²⁻⁶, unlike the binary FeSe with a maximum $T_c \sim 8$ K. This new $A_xFe_{2-y}Se_2$ (122)-type superconductor displays a large magnetic moment per Fe site, intrinsic Fe vacancy order in the ab -plane and an antiferromagnetic order in the c -direction^{7,8}. Several experiments have indicated that the superconductivity occurs only in Fe-deficient samples⁹⁻¹² and the ordering of Fe vacancies, important for their electronic and magnetic properties, can be controlled by heat treatments^{8,10,11,13-15}. In addition, the system is structurally phase separated at the nanoscale containing iron-vacancy ordered phase with an expanded in-plane lattice and a coexisting minority phase with compressed in-plane lattice¹³. Considering the complexity of the system it is of vital importance to investigate the coexisting phases for their electronic and magnetic properties.

In this work, we have exploited bulk-sensitive high energy spectroscopies to probe the coexisting electronic phases in the $K_{0.8}Fe_{1.6}Se_2$ superconductor. We have used

x-ray emission (XES) and high resolution x-ray absorption (XAS) spectroscopy to study the electronic and magnetic properties as a function of thermal cycling. Starting from room temperature (RT), where the system shows a nanoscale phase separation¹³, we have cooled the sample across the superconducting transition, and the temperature evolution of the electronic and magnetic properties is monitored while warming up to RT. Later, we have annealed the sample up to 606 K and quenched it down to 10 K for a direct comparison between as-grown and annealed samples. The results are discussed along with the electronic and magnetic properties of binary FeSe¹⁶ to distinctly identify the effect of K-intercalation on the electronic properties of these superconductors.

2. EXPERIMENTAL DETAILS

Measurements of XES and high resolution XAS were carried out on a well characterized as-grown single crystal of $K_{0.8}Fe_{1.6}Se_2$ ³. The experiments were performed at the beamline ID16 of the European Synchrotron Radiation Facility. The experimental setup consists of a spectrometer based on the simultaneous use of a bent analyzer Ge(620) crystal (bending radius $R=1$ m) and a pixelated position-sensitive Timepix detector¹⁷ in Rowland circle geometry. The scattering plane was horizontal and parallel to the linear polarization vector of the incident x-rays beam. The measurements were carried out fixing the sample surface (the ab -plane of the $K_{0.8}Fe_{1.6}Se_2$ single crystal) at $\sim 45^\circ$ from the incoming beam direction and the scattering angle 2θ at $\sim 90^\circ$. The total energy resolution was about 1.1 eV full width at half maximum. The samples were placed in a cryogenic environment and the temperature was controlled with an accuracy of ± 1 K.

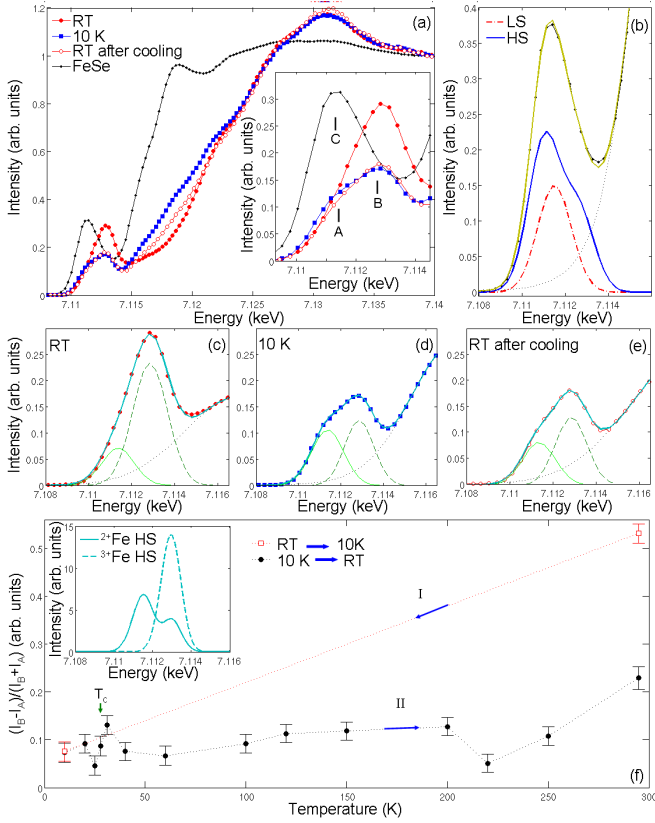


FIG. 1: (a) Partial fluorescence yield (PFY) spectra measured at the Fe K-edge of $\text{K}_{0.8}\text{Fe}_{1.6}\text{Se}_2$ at RT, 10 K, and RT after cooling, compared with the PFY spectrum of binary FeSe. The inset shows a zoom over the pre-peak region. (b) The pre-peak of FeSe is shown deconvoluted in two components representing the low (dot-dashed line) and high (solid line) spin ^{2+}Fe states. (c) - (e) The pre-peak of $\text{K}_{0.8}\text{Fe}_{1.6}\text{Se}_2$ is deconvoluted in two Gaussian features, A and B. (f) Temperature cycle of the relative intensities of the two features, $(I_B - I_A)/(I_B + I_A)$, while cooling down (I) followed by warming up to RT again (II). The inset represents theoretical simulation of the pre-edge region for tetrahedral high spin (HS) ^{2+}Fe (solid line) and ^{3+}Fe (dashed line) complexes¹⁹.

3. RESULTS AND DISCUSSIONS

Figure 1 (a) shows normalized Fe K-edge partial fluorescence yield (PFY) absorption spectra of $\text{K}_{0.8}\text{Fe}_{1.6}\text{Se}_2$, collected at different temperatures, obtained by collecting the Fe $\text{K}\beta_{1,3}$ emission intensity and scanning the incident energy across the absorption edge. The spectra are normalized with respect to the atomic absorption estimated by a linear fit far away from the absorption edge. The K-edge absorption process is mainly governed by the $1s \rightarrow \epsilon p$ dipole transition. In addition, the spectra show strong pre-peak features due to direct $1s \rightarrow 3d$ quadrupole transitions to the unoccupied Fe $3d$ hybridized with Se $4p$ states¹⁸. In the crystal-field picture the pre-peak is sensitive to the electronic structure and its energy position, splitting, and intensity distribution

change systematically with spin state, oxidation state, and local geometry¹⁹. The differences between the FeSe and the $\text{K}_{0.8}\text{Fe}_{1.6}\text{Se}_2$ are evident. The FeSe exhibits a broad and asymmetric single pre-peak feature C at $E_C \approx 7111.1$ eV (typical of ^{2+}Fe complexes²⁰) unlike $\text{K}_{0.8}\text{Fe}_{1.6}\text{Se}_2$, for which the pre-peak is composed by a doublet feature (see, e.g., the inset of Fig. 1 (a) showing a zoom over the pre-peak). The large width and asymmetry of the FeSe pre-peak feature indicates that this system may not be a simple low spin ^{2+}Fe complex, rather it should contain both low spin (LS) and high spin (HS) ^{2+}Fe states. Indeed, as shown in Fig. 1 (b), the FeSe pre-peak can be deconvoluted in two components due to LS and HS ^{2+}Fe states¹⁹. FeSe shows then an intermediate spin ^{2+}Fe state, consistent with the local Fe-moment of about $2 \mu_B$ ²¹. On the other hand, the PFY spectra of $\text{K}_{0.8}\text{Fe}_{1.6}\text{Se}_2$ apparently show a pre-peak with two features A and B, appearing at $E_A \approx 7111.4$ and $E_B \approx 7112.9$ eV. Since the system displays a large local Fe-moment of about $3.3 \mu_B$ ^{8,21,22} we expect a doubled absorption pre-peak to mainly represent the HS ^{2+}Fe state (however, with the more intense feature at lower energy as expected theoretically¹⁹). The fact that the spectral weight is higher at the higher energy, means that HS ^{3+}Fe state should coexist with HS ^{2+}Fe state (see, e.g., inset of Fig. 1 (f) showing calculated pre-peaks for tetrahedral HS ^{2+}Fe and ^{3+}Fe complexes). This constructs a direct evidence of coexisting electronic phases with different spin states in the $\text{K}_{0.8}\text{Fe}_{1.6}\text{Se}_2$ system.

Several experiments have revealed an intrinsic phase separation in the $\text{K}_{0.8}\text{Fe}_{1.6}\text{Se}_2$ system^{23–25} below ~ 580 K where iron vacancy-ordered structure is associated to the magnetic order^{8,27,28}. Alongwith the majority phase, a minority phase with slightly compressed in-plane lattice appears²³. It is likely that the two phases have different electronic properties due to local change of the Fe valence in different sublattices due to the high K mobility and distribution. In fact, the PFY spectra provide a clear evidence of electronic phase separation, consistent with the structural nematicity of the system. The in-plane compressed (out-of plane expanded) minority phase most likely corresponds to a ^{2+}Fe oxidation state, while the in-plane expanded (out-of plane compressed) phase with vacancy ordering to a ^{3+}Fe state. Despite the fact that the phase separation affects both in-plane and out-of-plane axes, the variation of the c -axis is 50% larger than that along the a, b directions. Consistently, the shift of the absorption edge reflects the fact that a c -axis expanded (compressed) phase corresponds to a lower (higher) energy.

In order to investigate the temperature evolution of the electronic phase separation, we have deconvoluted the pre-peak of $\text{K}_{0.8}\text{Fe}_{1.6}\text{Se}_2$ in two Gaussian features, A and B, with fixed energy positions (Fig. 1 (c)-(e)). A pseudo-Voigt function was used to describe the background due to the rising edge (dotted curve). The width of A has been kept fixed while that of B was variable to compensate the effect of the background subtraction. Fig-

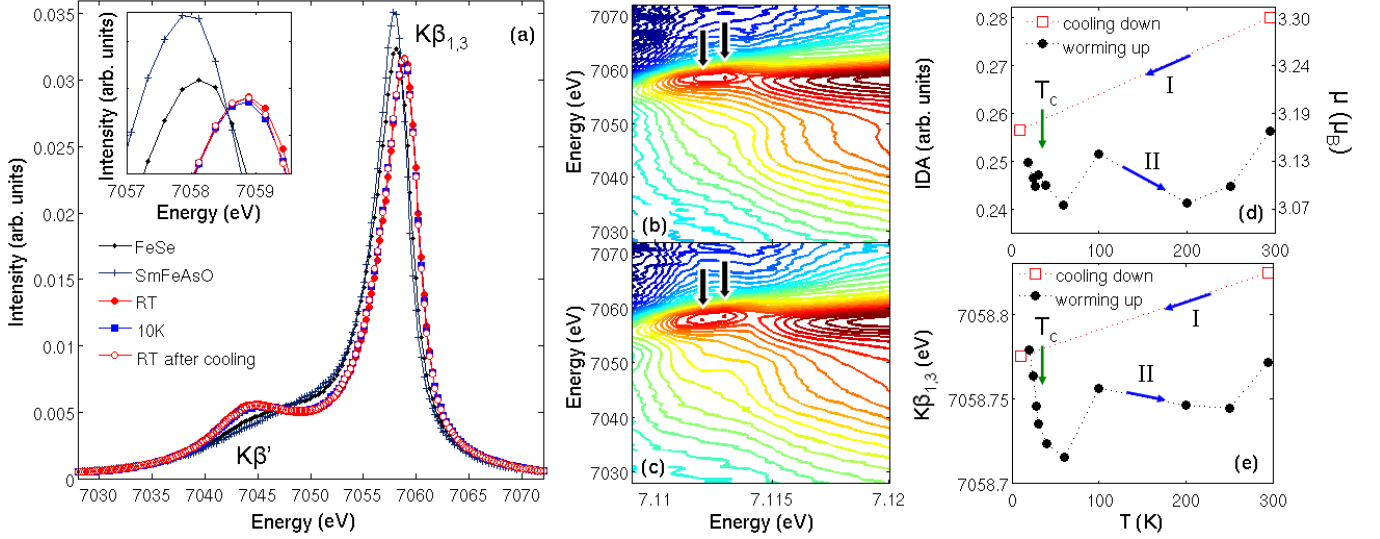


FIG. 2: (a) Fe $K\beta$ emission spectra of $K_{0.8}Fe_{1.6}Se_2$ at different temperatures, compared with the spectra measured on the FeSe and SmFeAsO. The spectra are normalized to the integrated area. The inset shows a zoom over the main $K\beta_{1,3}$ emission line. (b) and (c) Resonant x-ray emission maps at RT and 10 K respectively, measured at the $K\beta$ emission line with the incoming energy around the absorption pre-peak. The arrows indicate the two features resonating at E_A and E_B . (d) IDA as a function of temperature. Open squares represent the data while cooling down the sample (I) and the filled circles represent warming up from 10 K (II). The scale on the right hand side shows local magnetic moment (μ) determined following H. Gretarsson et al.²¹. (e) Energy position of the $K\beta_{1,3}$ main line as a function of temperature. The uncertainties are of the order of the symbols size.

ure 1 (f) displays relative intensity, $(I_B - I_A)/(I_B + I_A)$, representing the qualitative evolution of the coexisting electronic phases. Starting from RT and cooling down to 10 K, B loses and A gains intensity. This may be due to a reorganization between nanoscale phases while the sample is cooled. Warming up again to RT, differently from B, the feature A approximately recovers its initial intensity, however the distribution of the phases appears different. The temperature dependence of the relative intensity also reveals a small discontinuity across T_c . Moreover, a dome like anomaly is evident between 100 K to 220 K, similar to the resistivity anomaly seen in this system^{12,14,26,31}. It should be noticed that the Fe-Se bondlength does not show any change with temperature^{29,30}. This implies negligible change in the Fe 3d - Se 4p hybridization¹⁸. Therefore the absorption pre-peak, consisting HS 2^+Fe and HS 3^+Fe components, get redistributed without any appreciable effect of structural changes with temperature.

Independent and complementary information on the electronic and magnetic properties of the Fe 3d levels can be obtained from XES. Figure 2 (a) shows Fe $K\beta$ emission line measured on $K_{0.8}Fe_{1.6}Se_2$ at different temperatures along with the RT XES spectra of FeSe and SmFeAsO systems. In the crystal-field picture the overall spectral shape is dominated by the $(3p,3d)$ exchange interactions³². In particular, the presence (absence) of a pronounced feature at lower energy ($K\beta'$) is an indication of a HS (LS) state of Fe^{32} . Also, the energy position of the $K\beta_{1,3}$ provides information on the spin state reflecting the effective number of unpaired 3d electrons³².

Differences between the XES of $K_{0.8}Fe_{1.6}Se_2$, FeSe and SmFeAsO are evident.

In Fig. 2 (b) and (c) we have displayed the resonant x-ray emission maps collected at the Fe $K\beta$ emission with the incoming energy around the absorption pre-peak. The RT map in panel (b) shows a main feature and a shoulder, resonating at E_B and E_A respectively. The map measured at 10 K instead (panel (c)) reveals a clear enhancement of the shoulder intensity, appearing as a distinct feature at a lower emitted energy. This is a clear indication that the pre-peak feature A should be related to a lower spin state than feature B, in agreement with the hypothesis that features A and B correspond to HS 2^+Fe and 3^+Fe phases respectively. Therefore, the minority phase has reduced local Fe-moment with respect to the Fe-vacancy ordered phase. The observation further underlines the correlation between the Fe-vacancy order and local Fe-moment in the title system.

It is possible to quantify the local Fe-moment from the integrated area of absolute XES difference with respect to a LS reference²¹. Since SmFeAsO is almost non-magnetic²¹, we have taken SmFeAsO as a reference to obtain the integrated absolute difference (IDA), that is approximately proportional to the spin magnetic moment. In order to determine the relative variation in the magnetic moment, we have used the RT value of μ for $K_{0.8}Fe_{1.6}Se_2$ ($3.3 \mu_B$ ^{8,21,22}) and for FeSe ($2 \mu_B$ ²¹). Figure 2 (d) and (e) shows temperature dependence of the IDA and the energy position of the $K\beta_{1,3}$ main line. Since the two quantities provide the same information, qualitatively similar trends are observed. The changes

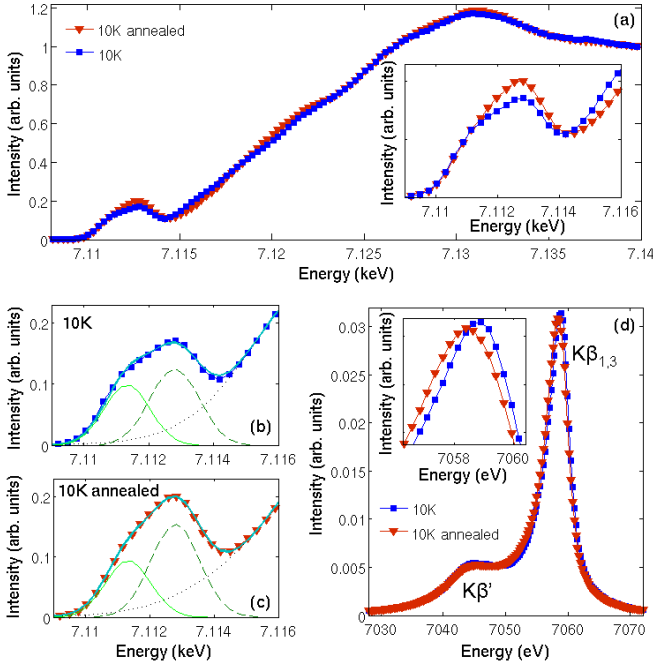


FIG. 3: (a) Partial fluorescence yield (PFY) spectrum at the Fe K-edge of $\text{K}_{0.8}\text{Fe}_{1.6}\text{Se}_2$ measured at 10K after high temperature annealing (triangles), compared with the PFY spectrum on as-grown (squares) sample. The inset shows the zoom over the pre-peak region. (b) and (c) the pre-peaks before and after annealing are shown deconvoluted in two Gaussian components. (d) Comparison of the Fe $\text{K}\beta$ emission spectra collected at 10 K on the sample as-grown (squares) and after the high temperature annealing (triangles).

in the $\text{K}\beta$ emission are very much consistent with those appearing in the absorption pre-peak, showing a reduced magnetic moment at low temperature due to the redistribution of the phases characterized by the HS ^{2+}Fe and HS ^{3+}Fe states. More quantitatively, cooling down, we observe a reduction of the local Fe-moment from 3.30 to $3.17 \mu_B$. Comparing the corresponding change in the PFY spectra, the reduction of the Fe-moment is too small if we consider the minority phase being in low-spin ^{2+}Fe with no local moment, confirming dominance of high-spin ^{2+}Fe state. In the temperature range from 10 K to 60 K, the μ continues to decrease down to a minimum of $3.08 \mu_B$, unlike a negligible change seen in the PFY. With further increase of temperature, the local Fe-moment μ appears to show dome shape anomalous variation around 150 K, that might be related with the resistivity anomaly^{12,14,26,31}. This kind of anomalous behavior can be expected from an inhomogeneous and glassy system with coexisting phases.

The glassy nature of the $\text{K}_{0.8}\text{Fe}_{1.6}\text{Se}_2$ is also evident from the effect of thermal cycling. To get further insight we have annealed the sample at 606 K for 20 minutes and quenched it down to 10 K. Figure 3 (a) shows the PFY

spectrum after this treatment, compared with the earlier one at 10 K. There is an apparent change in the pre-peak with the component B showing a relative increase after the annealing (Fig. 3 (b) and (c)). On the other hand, the $\text{K}\beta$ emission spectra reveals a clear decrease in the Fe-moment (Fig. 3 (d)). Indeed, the IDA for the annealed sample is ~ 0.187 , that corresponds to the $\mu \sim 2.79 \mu_B$ (to be compared with $\mu \sim 3.17 \mu_B$ for the as grown sample), more similar to the moment for the binary FeSe²¹. Therefore, the XES results are consistent with increase of lower spin ^{2+}Fe state by annealing. Apparently this is inconsistent with the PFY spectra in which the feature B has been assigned to high-spin ^{3+}Fe state. However, we should recall that the PFY of FeSe goes through a large change with pre-peak shifting towards higher energy under hydrostatic pressure³³ while the superconducting transition temperature changes from a low (8 K) to a high (37 K) value. Thus an intensity increase of the feature B in the PFY seems to be due to compressed low-spin ^{2+}Fe phase. Therefore, a distribution of different phases is likely, with even lower magnetic moment (most likely related with compressed FeSe filaments in the texture of the magnetic phase) that could be involved in the high T_c superconductivity of the $\text{K}_{0.8}\text{Fe}_{1.6}\text{Se}_2$ system. Indeed, the system is characterized by a large disorder and glassy local structure²⁹, similar to the granular materials.

4. CONCLUSIONS

In conclusion, we have investigated the evolution of the electronic and magnetic properties of $\text{K}_{0.8}\text{Fe}_{1.6}\text{Se}_2$ by XAS and XES measurements as a function of temperature in a close thermal cycle, providing a clear evidence of coexisting electronic phases characterized by different Fe valence and local magnetic moment. Using resonant XES we have found that the Fe-vacancy ordered (disordered compressed) phase corresponds to HS ^{3+}Fe (intermediate spin ^{2+}Fe). The presence of the HS ^{3+}Fe phase means that the minority superconducting phase is heavily electron doped, consistent with the absence of the hole pockets on the Fermi surface^{34,35}. We also find that the local Fe-moment sustains a substantial reduction under high temperature annealing due to disordering of the Fe vacancies. A comparative study with respect to the FeSe suggests that high T_c in the title system has a clear analogy with the increased T_c of binary FeSe under hydrostatic pressure. It looks like that the coexistence of different phases is the key, and since by annealing the disorder increases with a simultaneous decrease of the local Fe moment, it is likely that a fraction of different metallic compressed disordered phase in lower spin configuration²⁵ exists. These filamentary phases get superconducting as happens in the granular superconductors.

- ¹ Y. Mizuguchi, Y. Takano, J. Phys. Soc. Jpn. 79, 102001 (2010).
- ² Jiangang Guo, Shifeng Jin, Gang Wang, Shunchong Wang, Kaixing Zhu, Tingting Zhou, Meng He, and Xiaolong Chen, Phys. Rev. B 82, 180520 (2010).
- ³ Yoshikazu Mizuguchi, Hiroyuki Takeya, Yasuna Kawasaki, Toshinori Ozaki, Shunsuke Tsuda, Takahide Yamaguchi, and Yoshihiko Takano, Appl. Phys. Lett. 98, 042511 (2011).
- ⁴ J. J. Ying, X. F. Wang, X. G. Luo, A. F. Wang, M. Zhang, Y. J. Yan, Z. J. Xiang, R. H. Liu, P. Cheng, G. J. Ye, and X. H. Chen, Phys. Rev. B 83, 212502 (2011).
- ⁵ A Krzton-Maziopa, Z Shermadini, E Pomjakushina, V Pomjakushin, M Bendele, A Amato, R Khasanov, H Luetkens and K Conder, J. Phys.: Condens. Matter 23, 052203 (2011).
- ⁶ Ming-hu Fang, Hang-dong Wang, Chi-heng Dong, Zu-juan Li, Chun-mu Feng, Jian Chen and H. Q. Yuan, Europhys. Lett. 94, 27009 (2011).
- ⁷ D.H. Ryan, W.N. Rowan-Weetaluktuk, J.M. Cadogan, R. Hu, W.E. Straszheim, S.L. Budko, and P.C. Canfield, arXiv:1103.0059v1.
- ⁸ BAO Wei, HUANG Qing-Zhen, CHEN Gen-Fu, M. A. Green, WANG Du-Ming, HE Jun-Bao, QIU Yi-Ming, Chin. Phys. Lett. 28, 086104 (2011).
- ⁹ Jing Guo, Xiaojia Chen, Chao Zhang, Jiangang Guo, Xiaolong Chen, Qi Wu, Dachun Gu, Peiwen Gao, Xi Dai, Lihong Yang, Ho-kwang Mao, Liling Sun, Zhongxian Zhao, arXiv: 1101.0092; Y. Kawasaki, Y. Mizuguchi, K. Deguchi, T. Watanabe, T. Ozaki, S. Tsuda, T. Yamaguchi, Hiroyuki Takeya, Y. Takano, arXiv: 1101.0896; J J Ying, X F Wang, X G Luo, Z Y Li, Y J Yan, M Zhang, A F Wang, P Cheng, G J Ye, Z J Xiang, R H Liu and X H Chen, New J. Phys. 13, 033008 (2011).
- ¹⁰ D. M. Wang, J. B. He, T.-L. Xia, and G. F. Chen, Phys. Rev. B 83, 132502 (2011).
- ¹¹ A. M. Zhang, J. H. Xiao, J. B. He, D. M. Wang, G. F. Chen, Q. M. Zhang, arXiv: 1101.2168v1.
- ¹² Y. J. Yan, M. Zhang, A. F. Wang, J. J. Ying, Z. Y. Li, W. Qin, X. G. Luo, J. Q. Li, Jiangping Hu, X. H. Chen, Scientific Reports 2, Article number: 212 (2012).
- ¹³ Alessandro Ricci, Nicola Poccia, Bobby Joseph, Gianmichele Arrighetti, Luisa Barba, Jasper Plaisier, Gaetano Campi, Yoshikazu Mizuguchi, Hiroyuki Takeya, Yoshihiko Takano, Naurang Lal Saini and Antonio Bianconi, Supercond. Sci. Technol. 24, 082002 (2011).
- ¹⁴ Fei Han, Bing Shen, Zhen-Yu Wang, Hai-Hu Wen, arXiv:11031347v1.
- ¹⁵ V. Svitlyk, D. Chernyshov, E. Pomjakushina, A. Krzton-Maziopa, K. Conder, V. Pomjakushin, and V. Dmitriev, Inorg. Chem. 50, 10703 (2011).
- ¹⁶ L. Simonelli, N.L Saini, Y. Mizuguchi, Y. Takano, T. Mizokawa, G. Baldi, and G. Monaco, submitted to Europhysics Letters.
- ¹⁷ C Ponchut, J M Rigal, J Clment, E Papillon, A Homs and S Petitdemange, Journal of Instrumentation 6, C01069 (2011).
- ¹⁸ B Joseph, A Iadecola, L Simonelli, Y Mizuguchi, Y Takano, T Mizokawa, and N L Saini, J. Phys.: Condens. Matter 22, 485702 (2010).
- ¹⁹ Tami E. Westre, Pierre Kennepohl, Jane G. DeWitt, Britt Hedman, Keith O. Hodgson, and Edward I. Solomon, J. Am. Chem. Soc. 119, 6297 (1997).
- ²⁰ B. C. Chang, Y. B. You, T. J. Shiu, M. F. Tai, and H. C. Ku, Y. Y. Hsu, L. Y. Jang and J. F. Lee, Z. Wei, K. Q. Ruan, and X. G. Li, Phys. Rev. B 80, 165108 (2009); Ignatov A, Zhang C L, Vannucci M, Croft M, Tyson T A, Kwok D, Qin Z and Cheong S-W, arXiv:0808.2134v2.
- ²¹ H. Gretarsson, A. Lupascu, Jungho Kim, D. Casa, T. Gog, W. Wu, S. R. Julian, Z. J. Xu, J. S. Wen, G. D. Gu, R. H. Yuan, Z. G. Chen, N.-L. Wang, S. Khim, K. H. Kim, M. Ishikado, I. Jarrige, S. Shamoto, J.-H. Chu, I. R. Fisher, Young-June Kim, arXiv:1107.2211v1.
- ²² Xun-Wang Yan, Miao Gao, Zhong-Yi LU, Tao Xiang, arXiv:1102.2215v1.
- ²³ A. Ricci, N. Poccia, G. Campi, B. Joseph, G. Arrighetti, L. Barba, M. Reynolds, M. Burghammer, H. Takeya, Y. Mizuguchi, Y. Takano, M. Colapietro, N. L. Saini, and A. Bianconi, Phys. Rev. B 84, 060511(R) (2011).
- ²⁴ Z. Wang, Y. J. Song, H. L. Shi, Z. W. Wang, Z. Chen, H. F. Tian, G. F. Chen, J. G. Guo, H. X. Yang, and J. Q. Li, Phys. Rev. B 83, 140505(R) (2011).
- ²⁵ F. Chen, M. Xu, Q. Q. Ge, Y. Zhang, Z. R. Ye, L. X. Yang, Juan Jiang, B. P. Xie, R. C. Che, M. Zhang, A. F. Wang, X. H. Chen, D. W. Shen, X. M. Xie, M. H. Jiang, J. P. Hu, D. L. Feng, Phys. Rev. X 1, 021020 (2011).
- ²⁶ Wei Bao, G. N. Li, Q. Huang, G. F. Chen, J. B. He, M. A. Green, Y. Qiu, D. M. Wang, J. L. Luo, Materials Science 233, 1(2011).
- ²⁷ Z. Shermadini, A. Krzton-Maziopa, M. Bendele, R. Khasanov, H. Luetkens, K. Conder, E. Pomjakushina, S. Weyeneth, V. Pomjakushin, O. Bossen, and A. Amato, Phys. Rev. Lett. 106, 117602 (2011); V. Yu. Pomjakushin, D. V. Sheptyakov, E. V. Pomjakushina, A. K. Maziopa, K. Conder, D. Chernyshov, V. Svitlyk, and Z. Shermadini, Phys. Rev. B 83, 144410 (2011).
- ²⁸ R. H. Liu, X. G. Luo, M. Zhang, A. F. Wang, J. J. Ying, X. F. Wang, Y. J. Yan, Z. J. Xiang, P. Cheng, G. J. Ye, Z. Y. Li and X. H. Chen, Europhys. Lett. 94, 27008 (2011).
- ²⁹ A. Iadecola, B. Joseph, L. Simonelli, A. Puri, Y. Mizuguchi, H. Takeya, Y. Takano, N. L. Saini, J. Phys.: Condens. Matter 24, 115701 (2012).
- ³⁰ T. A. Tyson, T. Yu, S. J. Han, M. Croft, G. D. Gu, I. K. Dimitrov, and Q. Li, Phys. Rev. B 85 024504 (2012).
- ³¹ Ming-Hu Fang, Hang-Dong Wang, Chi-Heng Dong, Zu-Juan Li, Chun-Mu Feng, Jian Chen and H. Q. Yuan, Europhys. Lett. 94, 27009 (2011).
- ³² P. Glatzel and Uwe Bergmann, Coordination Chemistry Reviews 249, 65 (2005).
- ³³ J. M. Chen, S. C. Haw, J. M. Lee, T. L. Chou, S. A. Chen, K. T. Lu, Y. C. Liang, Y. C. Lee, N. Hiraoka, H. Ishii, K. D. Tsuei, Eugene Huang, and T. J. Yang, Phys. Rev. B 84, 125117 (2011).
- ³⁴ Lin Zhao, Daixiang Mou, Shanyu Liu, Xiaowen Jia, Junfeng He, Yingying Peng, Li Yu, Xu Liu, Guodong Liu, Shaolong He, Xiaoli Dong, Jun Zhang, J. B. He, D. M. Wang, G. F. Chen, J. G. Guo, X. L. Chen, Xiaoyang Wang, Qinqun Peng, Zhimin Wang, Shenjin Zhang, Feng Yang, Zuyan Xu, Chuangtian Chen, and X. J. Zhou, Phys. Rev. B 83, 140508 (2011).
- ³⁵ T. Qian, X.-P. Wang, W.-C. Jin, P. Zhang, P. Richard, G. Xu, X. Dai, Z. Fang, J.-G. Guo, X.-L. Chen, and H. Ding,

Phys. Rev. Lett. 106, 187001 (2011).